ADVANCED MATERIALS INTERFACES
www.advmatinterfaces.de

Underwater Superaerophobicity/Superaerophilicity and Unidirectional Bubble Passage Based on the Femtosecond Laser-Structured Stainless Steel Mesh

Jinglan Huo, Qing Yang, Jiale Yong, Peixun Fan, Yongfeng Lu, Xun Hou, and Feng Chen**

To control the behavior of underwater bubbles, stainless steel meshes are treated through femtosecond laser processing, and the bubble absorption, bubble interception, and unidirectional bubble passage are realized by using structured meshes. The surface of the mesh presents a micro–sub-micro–nano trinary-scale structure (microscale mesh wires, sub-microripples, and nanoparticles) after one-step laser ablation on both sides. The surface shows superhydrophilic in air and superaerophobic once immersed in water. After further modified with fluoroalkylsilane, the wettability of the sample surface is switched to be superaerophilic in water with bubble being absorbed by the sample. When a plenty of underwater bubbles arrive at the structured stainless steel mesh surface, they can be blocked by the underwater superaerophobic mesh but pass through the underwater superaerophilic mesh. In addition, after the mesh being treated only one side and further modified, it is to be Janus mesh and presents asymmetrical wettability of aerophilicity/superaerophilicity. The Janus mesh shows the unidirectional passage of underwater bubbles. Bubbles can only penetrate from aerophilic side to superaerophilic side, but be blocked from the other direction. The mesh is verified to be used to eliminate the stuck bubbles in the container.

1. Introduction

The bubbles in aqueous environment play a very important role in our lives and productions, such as the gas evolution reactions,[1–3] improving the flotation recovery of fine mineral particles,[4–6] collecting useful gas like methane or harmful gas like toxic sulfide gas in water.[7,8] Meanwhile, the bubbles also do harm in microfluidic field, which increase the fluid frictional and cause cultured cell death,[9–12] and in gas-generating electrochemical reaction process in which the generated bubbles stick on the electrode and account for the reduction of the reaction efficiency.[13,14] Hence, bubble manipulation could foster strengths and circumvent weaknesses of underwater bubbles' unbridled behaviors and have received fevered attention.[15–19] The underwater bubble manipulation in the aspect of superwettability transition[20–29] and unidirectional transportation relying on the substrate with extreme wettability attracts a plenty of researches.[30–33] Yong et al. prepared $Cu(OH)_2$ nanoneedles on a copper mesh by the immersion of the copper mesh in $NaOH/(NH_4)S_2O_8$ solution.[20] The nanoneedle-structured mesh is underwater superaerophobic and has the ability of gas interception in water. After modified with fluoroalkylsilane, the resultant mesh exhibits underwater superaerophobicity and could absorb underwater gas bubbles. Huo et al. realized the reversible transition between underwater superaerophilicity and superaerophobicity on the femtosecond laser-induced rough polytetrafluoroethylene (PTFE) surface by vacuum-pumping treatment.[21] The structured superaerophilic PTFE sheet could switch to be superaerophobic in water derived from its structures being wetted and filled by the water under external pressure produced by vacuum pumping. Yong et al. reported the superwettability transition of underwater bubbles on the femtosecond laser-structured polydimethylsiloxane (PDMS) polymer sheet through oxygen plasma irradiation.[22] By inducing hydrophilic group, silanol radical groups (—SiOH), onto the laser-induced rough PDMS surface, the original underwater superaerophilicity of structured PDMS sheet transformed into underwater superaerophobicity. Although these reports could control the bubble behavior in water on the chosen substrates, the controls of bubble were homogeneous in cross-sectional direction that limits the applications of the resulted sample. Janus substrates that described the asymmetric bubble behavior on upper and lower surfaces made improvements to those symmetrical substrates.[30–32] Jiang et al. fabricated

Dr. J. Huo, Dr. J. Yong, Prof. X. Hou, Prof. F. Chen
State Key Laboratory for Manufacturing System Engineering and Shaanxi Key Laboratory of Photonics Technology for Information
School of Electronics & Information Engineering
Xi'an Jiaotong University
Xi'an 710049, P. R. China
E-mail: jlyong@xjtu.edu.cn; chenfeng@mail.xjtu.edu.cn
Prof. Q. Yang
School of Mechanical Engineering
Xi'an Jiaotong University
Xi'an 710049, P. R. China
Dr. P. Fan, Prof. Y. Lu
Department of Electrical and Computer Engineering
University of Nebraska-Lincoln
Lincoln, NE 68588, USA
The ORCID identification number(s) for the author(s) of this article can be found under https://doi.org/10.1002/admi.201902128.

DOI: 10.1002/admi.201902128

an integrated Janus mesh called "bubble diode" by bonding superaerophobic and aerophilic single-layer copper meshes.[33] Gas bubbles could pass though the integrated Janus mesh from the superaerophobic side but be blocked from the aerophilic side. However, the process of preparing two single layers separately by chemically etching and then bonding them might be complex and not flexible. Femtosecond laser ablation has the ability to texture almost all of the known materials and fabricate the micro/nanostructures to construct the extreme wettability surfaces through a simple one-step ablation processing.[31–39] Wu and co-workers prepared a superhydrophobic/hydrophilic Janus aluminum and zinc foil by femtosecond laser drilling.[31,32] The tapered through micropores array produced a self-driving force on air bubbles to let bubbles penetrate unidirectionally. However, subject to the limited pulse energy and repetition frequency, the drilling process to prepare through holes one by one is time consuming.

Here, we realized the underwater superaerophobicity, underwater superaerophilicity, and unidirectional bubble transportation on stainless steel mesh by the combination of one-step femtosecond laser ablation and fluoroalkylsilane modification. After the laser scanning on both sides of stainless steel mesh, the increase of mesh surface roughness and the surface oxidation endowed the stainless steel mesh with superhydrophilicity in air and superaerophobicity in water. Further modified with low-surface-energy fluoroalkyl by immersing in ethanol solution of fluoroalkylsilane, the wettability of rough mesh changed thoroughly to be superhydrophobic in air and underwater superaerophilic. In addition, a Janus mesh with underwater superaerophilicity/aerophilicity was directly fabricated by femtosecond laser treating only one side of the mesh. Underwater bubbles penetrated from the unstructured aerophilic side to structured superaerophilic side, but were blocked from the opposite direction. The Janus stainless steel mesh was then used as a "diode membrane" to eliminate the adhered bubbles at the bottom of the tank and collect them into the small tube.

2. Results and Discussion

2.1. Surface Microstructure

The stainless steel mesh was directly ablated by focused femtosecond laser beam to generate surface microstructure (**Figure 1**a,b). Then, the structured stainless steel mesh was immersed in fluoroalkyl silane at room temperature to reduce the free energy of the mesh surface (Figure 1c).

The wire surface of a bare stainless steel mesh is smooth and clean without particles covering on it (**Figure 2**a). In contrast, nanostructure was created on the wire surface by femtosecond laser processing. Figure 2b,c shows the scanning electron microscope (SEM) images of a stainless steel mesh whose surface was ablated by femtosecond laser at the scanning speed of 4 mm s^{-1} and the scanning space of 4 μm. The wire surface of the ablated mesh is covered with typical laser-induced periodic sub-micrometer ripples with the period of 0.7 μm (Figure 2b). The formation of periodic ripples has been accepted as a universal phenomenon caused by the interference between the incident laser beam and the scattered one under femtosecond laser processing. The spatial period is usually close to the laser wavelength.[40–42] Meanwhile, there are a mass of nanoparticles with sizes of tens of nanometers decorating on the surfaces of the nanoripples (Figure 2c). They may be caused by the spot fringe ablation with low fluence during the laser spot moving.[43,44] When irradiated by femtosecond pulses at intensities around the threshold for plasma formation, the ejection of matter always leads to the formation of the nanoparticles of the target material.[45] As a result, a trinary-scale structures (microscale mesh wires, sub-microripples, and nanoparticles) formed on the mesh after one-step femtosecond laser ablation. When the laser scanning speed is larger than 4 mm s^{-1} and the scanning space is larger than 4 μm, only plenty of nanoscale particles were induced on the entire mesh surface without ripples structure (Figure S1, Supporting Information).

Figure 3 shows the energy-dispersive X-ray (EDX) results of different stainless steel mesh. In comparison to the original stainless steel mesh (Figure 3a), after femtosecond laser ablation, new O element at the peak of 0.525 eV appeared (Figure 3b), indicating that oxidation occurred simultaneously with the formation of multilevel microstructure during the laser ablation process. As the laser-structured surface was further lowered surface free energy by fluoroalkylsilane modification, a monolayer of fluoroalkylsilane was successfully coated on the sample surface. As a verification, F element at the peak of 0.677 eV was detected on the fluoroalkylsilane-modified surface (Figure 3c). Meanwhile, the laser-induced structures did not change after modification treatment (Figure S2, Supporting

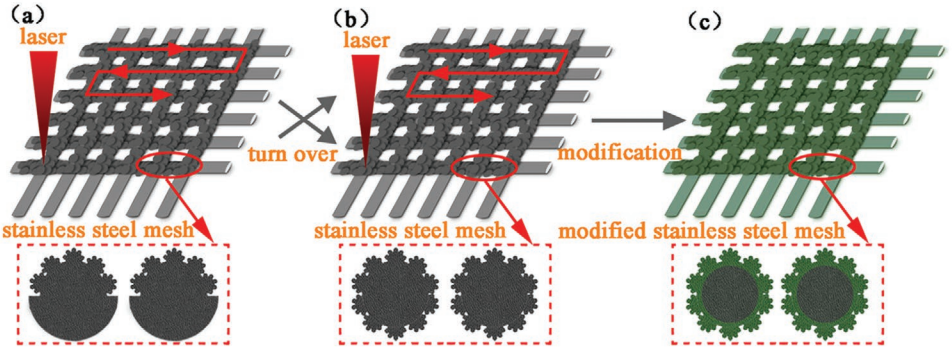

Figure 1. a–c) The procedure Schematic of fabricating the superhydrophilic/underwater superaerophobic and superhydrophobic/underwater superaerophilic stainless steel mesh by femtosecond laser ablation.

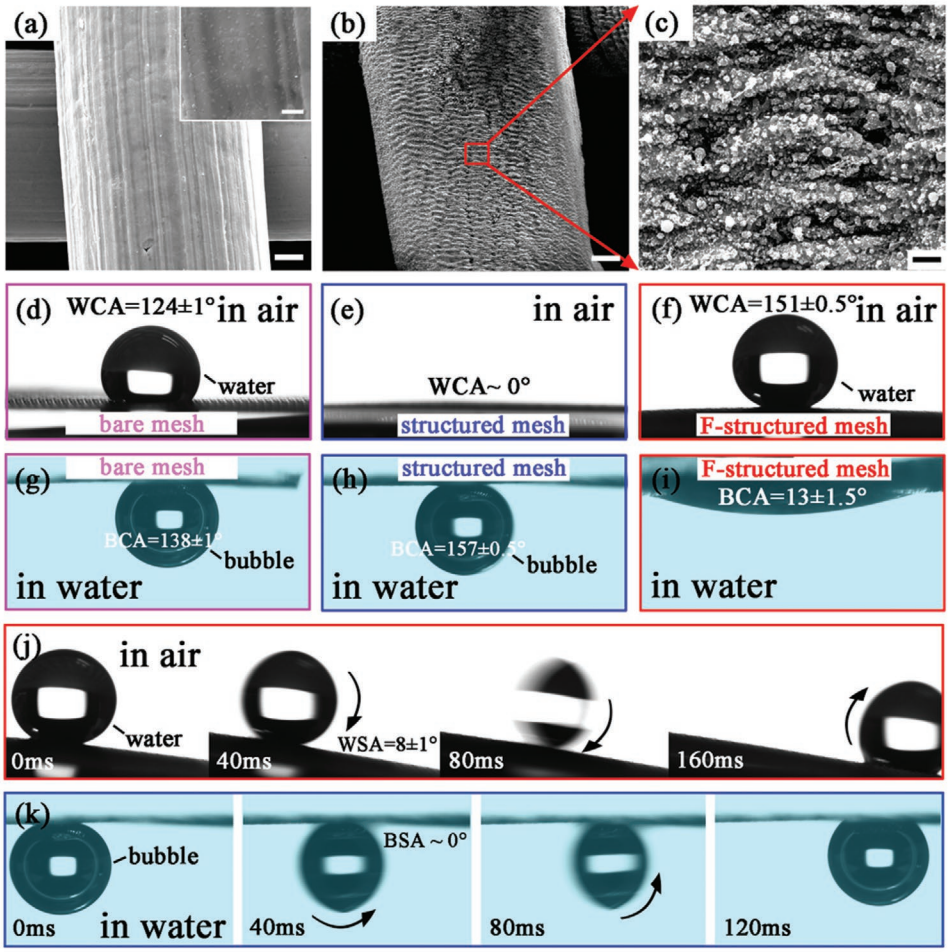

Figure 2. The morphology and wettability characterization of unstructured bare and laser-structured rough stainless steel meshes. a–c) SEM images of a) bare stainless steel mesh with magnification times of 5000× and 50 000× and b,c) both-side structured stainless steel mesh with magnification times of 5000× and 50 000×. It is obvious that after laser ablation the smooth microwire was covered with sub-microripples and nanoparticles. d–f) WCAs on bare, structured, and structured fluorinated stainless steel meshes, respectively. g–i) Underwater BCAs on bare, structured, and structured fluorinated stainless steel meshes, respectively. j) Water droplet rolled away easily on the structured fluorinated stainless steel mesh with a WSA of 8° ± 1°. k) An underwater bubble rolled away easily along the structured stainless steel mesh with the BSA nearly of 0°. Scale bars in figure (a) and its inset image and in figure (b) and c) are 10, 1, 10, and 1 µm, respectively.

Information). For convenience, the laser-treated stainless steel mesh with trinary-scale rough microstructures was defined as "structured mesh," and the fluorinated rough stainless steel mesh was defined as "F-structured mesh."

2.2. Underwater Bubble Wettability

When a water droplet was placed on the original untreated stainless steel mesh, the water contact angle (WCA) was measured

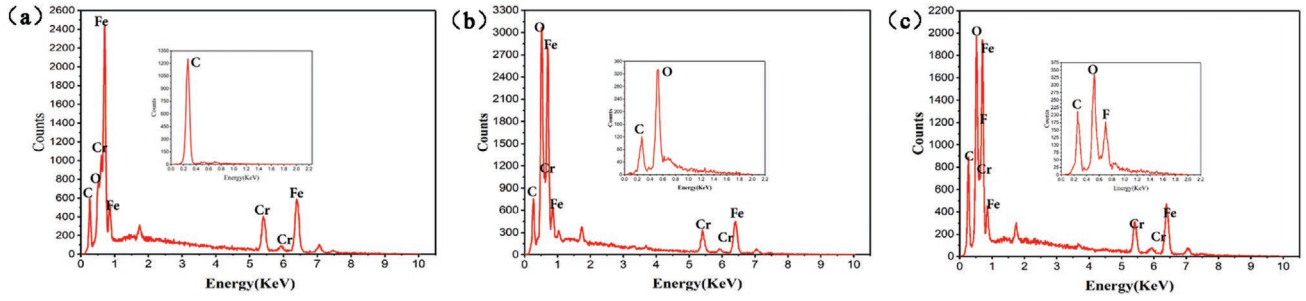

Figure 3. Surface elements of different stainless steel meshes: a) the untreated bare mesh, b) the laser-structured mesh, and c) the F-structured mesh. The insets are corresponding EDX images with the low excitation voltage of 2 kV.

as 124° ± 1°, which presents the intrinsic hydrophobicity of the bare mesh (Figure 2d). The hydrophobic property of the stainless steel mesh is caused by its original microscale porous structure, which results in a discontinuous three-phase contact line at the water–solid contact interface. As the untreated mesh was dipped into water, a bubble exhibited quasispherical shape with the bubble contact angle (BCA) of 138° ± 1° on the mesh surface, so the bare mesh shows underwater aerophobicity (Figure 2g). The laser-induced trinary-scale rough microstructures change the stainless steel mesh from hydrophobic to superhydrophilic. When a water droplet was dripped onto the structured mesh surface in air, it spread out quickly and looked like being absorbed by the mesh finally. The WCA of this droplet is nearly 0° (Figure 2e). In a water medium, the bubble was greatly repelled by the structured mesh and could maintain a stable spherical shape with the BCA of 157° ± 0.5° on the mesh (Figure 2h). If the sample was slightly tilted, the bubble would roll away easily along the sample surface (Figure 2k), demonstrating excellent superaerophobicity and ultralow adhesion of the structured mesh to underwater bubbles. The fluoroalkylsilane modification dramatically decreases the free energy of the rough mesh surface. The F-structured mesh is superhydrophobic in air. A water droplet on such surface was able to keep a spherical shape with the WCA of 151° ± 0.5° (Figure 2f) and roll off easily with the water sliding angle (WSA) of 8° ± 1° (Figure 2j). The underwater bubble on the F-structured mesh had a completely opposite behavior compared to that on the structured mesh. As long as the bubble was in contact with the F-structured mesh in water, the bubble was absorbed by the mesh within 20 ms, resulting in a small BCA of 13° ± 1.5°. This fast absorption process reveals that the F-structured mesh showed underwater quasi-superaerophilicity.

Figure 4 reveals the formation mechanism of the underwater superaerophobicity of the structured mesh and the quasi-superaerophilicity of the F-structured mesh. Whether a trapped air layer between water and rough surface exists or not has an important influence on the underwater bubble behavior on different meshes.[21] Femtosecond laser processing not only constructed the microstructure on stainless steel mesh surface but also changed the chemical elements. The increase of surface roughness and atomic proportion of O resulted in the superhydrophilicity of structured mesh surface.[34] When a water droplet was dripped on the structured mesh, the droplet spread out promptly. The water wets the surface microstructure thoroughly at the Wenzel contact state (Figure 4a). After the immersion of the structured mesh in water, both the micropores and rough structures of the mesh were filled with water, forming a water/solid composite interface (Figure 4b). When a bubble was placed on the mesh surface in water, it could only contact with the tips of the surface microstructure. Tiny contact area and natural bubble repellence of water together resulted in an underwater Cassie–Baxter contact state between the bubble and structured mesh, in which bubble maintained a spherical shape over time (Figure 4c,d). Conversely, after fluoroalkylsilane modification, the wettability of the F-structured mesh switched from superhydrophilicity to superhydrophobicity. A water droplet on the mesh surface is unable to wet into the space of microstructures, in agreement with the Cassie–Baxter contact state in air (Figure 4e). As the F-structured mesh was immersed in water, a trapped air layer appeared surrounding the mesh and filled the microphores and rough structures of the mesh (Figure 4f). Once a released bubble reached to the mesh surface, pressure difference inside and outside the bubble pushed the bubble to merge with the pre-existed air layer (Figure 4g). The bubble spread out along the gas/solid interface, giving rise to underwater superaerophilicity for the F-structured mesh (Figure 4h).

2.3. Selective Passage of Bubbles

The influence of underwater bubble wettability of mesh surface on the bubbles passage was investigated (**Figure 5**). When continuous bubbles were released blow the submersed structured mesh, they floated upward with buoyancy. As they first touched the mesh surface, they bounced up and then mixed with next rising bubble. Finally, the merged bigger bubble rolled away from the mesh edge (Figure 5a,b). That is, the laser-induced structured stainless steel mesh could prevent bubbles passing through without any gas leaving in sample, revealing its favorable antibubble capability. As for the F-structured mesh surface, owning to its superaerophilicity in water, the continuous bubbles contacted, spread out, and were absorbed by it to form a large air pocket. With the increase of the volume of air pocket, the mesh pores were forced by Laplace pressure difference and could not sustain this increasing pocket. Trapped

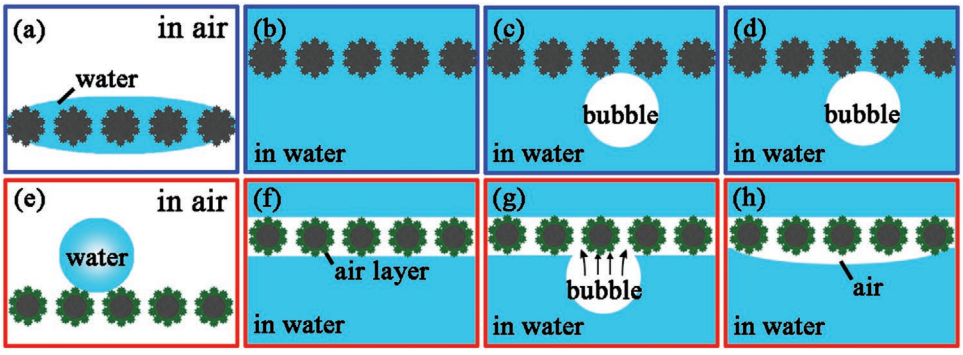

Figure 4. The internal mechanism of a–d) underwater superaerophobicity on structured mesh surface and e–h) underwater superaerophilicity on F-structured mesh surface.

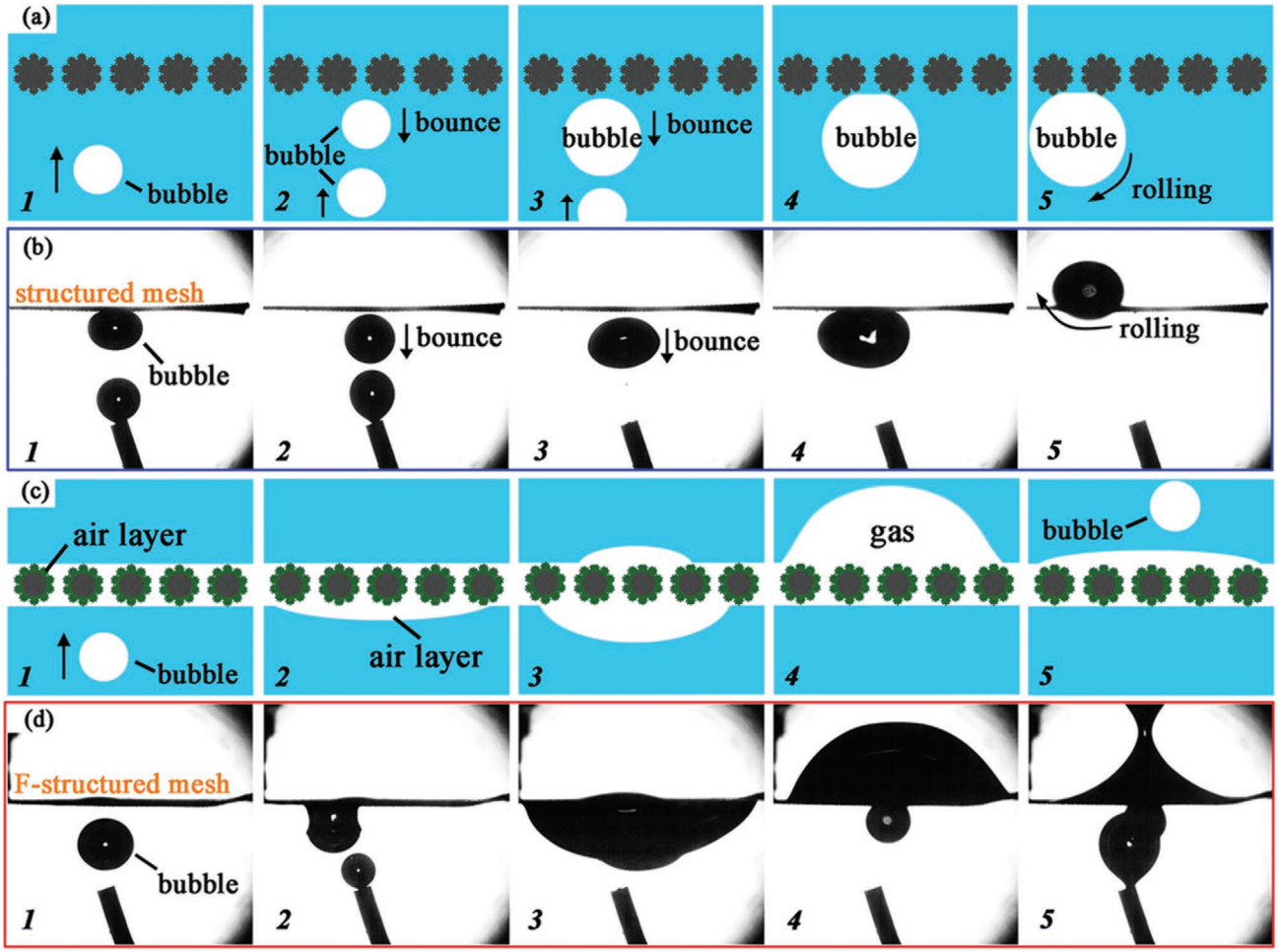

Figure 5. Dynamic selective passage of underwater bubbles through structured rough stainless steel mesh surface without or with fluoroalkylsilane modification. a,b) Schematic illustration and Snapshots process of underwater bubbles being intercepted by structured mesh. c,d) Schematic illustration and Snapshots process of underwater bubbles being absorbed and passed through the F-structured mesh.

gas bulged upward in a moment due to its own buoyancy, and finally overflowed upward the surface (Figure 5c,d). In stark contrast with the former structured mesh without fluoroalkylsilane modification, the F-structured stainless steel mesh surface could grab the bubbles and let them go, revealing its bubble-collecting capability. The underwater bubble selective passage of femtosecond laser-induced stainless steel with or without reducing surface energy treatment has application prospect in the fields of microfluidics.

2.4. Janus Mesh

In a quest to integrate the bubble selective passage property on one same sample to realize the unidirectional passage, the monolateral F-structured mesh (defined as MF-structured mesh) was fabricated by combing the femtosecond laser ablation and fluoroalkylsilane modification. Usually, the unidirectional passage of bubble occurs on the Janus mesh, whose wettabilities of top and bottom sides are different. The key factor is trapping the different air layer in water environment on different sides in order to realize the wetting gradient on the cross-sectional direction. Here, femtosecond laser was used to texture one side surface based on the "line-by-line" scanning method to form the monolateral structured mesh (defined as M-structured mesh). Scanning speed and scanning interval were 4000 μm s^{-1} and 4 μm, respectively. Straight after that, the M-structured mesh was dipped in the mixed fluorosilane–ethanol solution for 24 h to form an MF-structured mesh with one side of rough/low-energy property and one side of flat/low-energy property (**Figure 6**a). The rough/low-energy side exhibited superhydrophobicity and underwater superaerophilicity, while the flat/low-energy side exhibited hydrophobicity and underwater aerophilicity. The WCA and BCA on the stainless steel mesh that both sides were flat and low energy were measured with 140° and 78°, respectively (Figure 6b). Once immersed in water, the structured fluorinated side (S-F side) trapped an air layer, while the unstructured fluorinated side (US-F side) could not trap the air layer. The as-prepared mesh could be regarded as the Janus mesh.

Immersing the Janus mesh into water, when the aerophilic side (that is US-F side) was downward, the continuous supplied

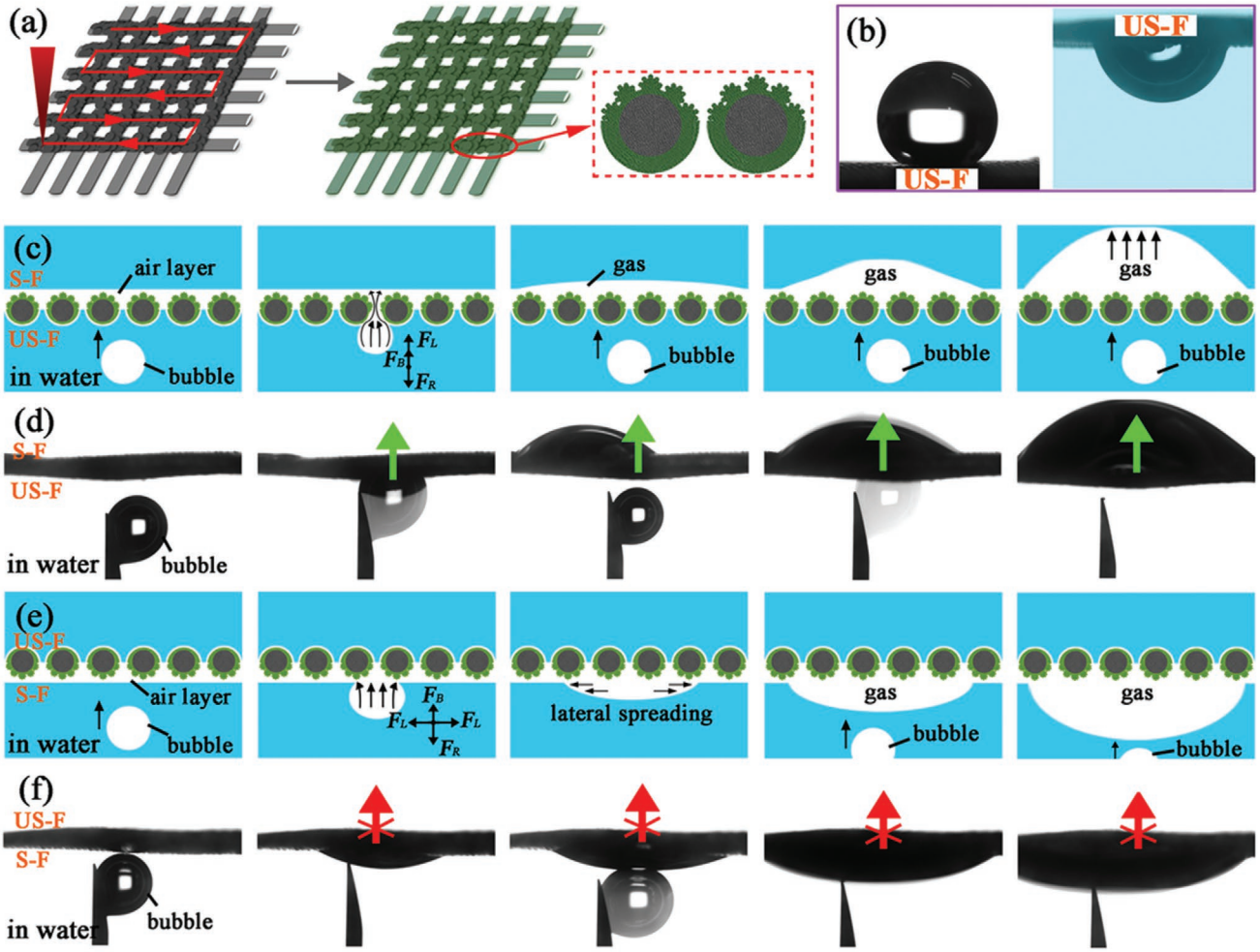

Figure 6. Fabrication process and bubble wettability characterization of Janus stainless steel mesh. a) Schematic illustration of Janus mesh fabrication. b) WCA and BCA of unstructured fluorinated mesh surface (US-F surface). c,d) Schematic illustration and Snapshots process of underwater bubbles passing through the Janus mesh surface from US-F side to S-F side. e,f) Schematic illustration and Snapshots process of underwater bubbles being intercepted once moving from S-F side to US-F side.

bubbles contacted the US-F surface first and then were inhaled to top surface rapidly one by one. That is, the bubbles were allowed to pass through the MF-structured mesh and gathered to a bulged air pocket (Figure 6c,d). It was just like "turning on" a bubble switch on this direction. On the contrary, once turn over the sample mesh in water, the bubbles contacted S-F surface first. Because of the superaerophilicity of S-F surface, continuous bubbles spread out along it and were intercepted by the top water layer so that they could not pass through mesh (Figure 6e,f). It could be regarded as "turning off" the bubble switch on this direction.

The mechanism of unidirectional transportation is depicted in Figure 6c,e. For the situation of bubbles contacting US-F surface first (Figure 6c), the bubble suffers three forces at this moment: upward buoyancy (F_B), upward Laplace force (F_L), and downward resistance force (F_R). The US-F surface could trap a "thin air layer" because of its hydrophobicity. The bubble, the "thin air layer," and the thick air layer trapped in the S-F surface make up a gas channel where bubble and as-existing air layer are connected. According to the Young–Laplace equation, the Laplace pressure difference is large enough (for the reason of small bubble curvature radius) to generate a F_L greatly overcoming F_R. So the bubbles chose to pass through and spread out on S-F surface instead of stop on the surface. In addition, in order to verify F_L further larger than F_B and F_R, the bubbles were operated contacting US-F surface from top, they still penetrated downward as well (Figure S3, Supporting Information). As for the situation of bubbles contacting S-F surface first (Figure 6e), a bubble suffers upward F_B, downward F_R, and F_L along the lateral direction. Under such circumstances, bubbles tended to directly spread out on S-F surface and could not connect with top US-F surface, in which case F_B and F_R kept balance. As a result, bubbles chose to spread and gathered on S-F surface instead of penetrating the mesh. To sum, bubbles could realize unidirectional transport on the MF-structured stainless steel mesh. During the process, the position of trapped air layer played the most important role. Touching the trapped air layer first made bubbles to spread and be obstructed, whereas the bubble penetrated the mesh rapidly while first touching the opposite side without trapped air layer.

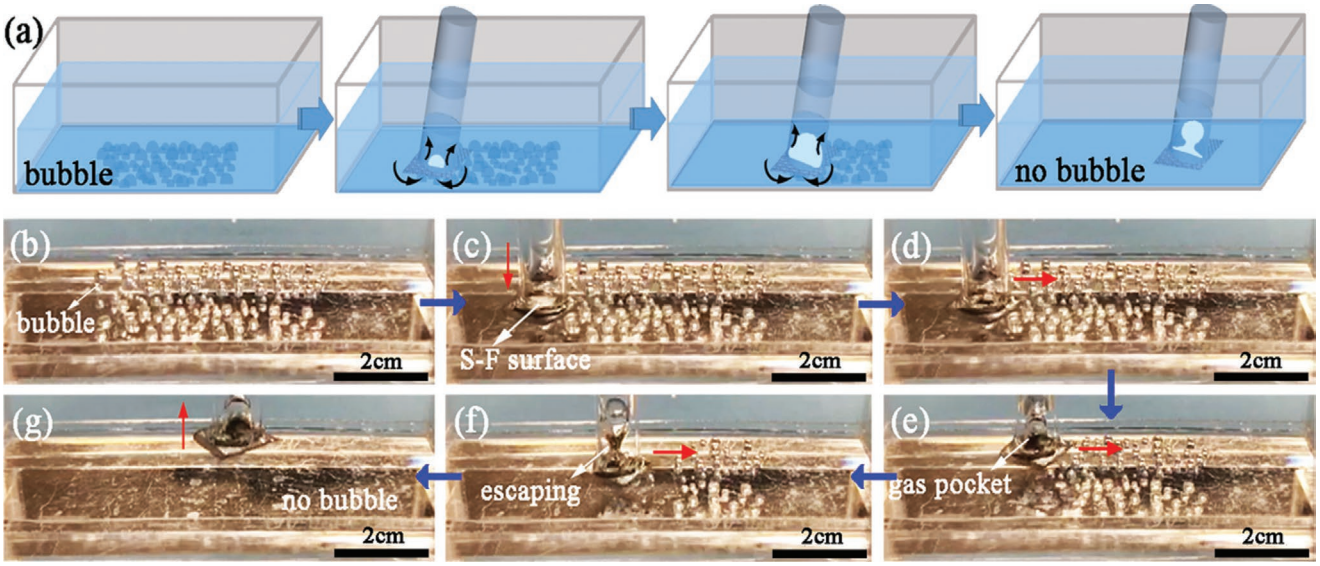

Figure 7. The clearance and collection of underwater bubbles using the Janus stainless steel mesh. a) Schematic illustration of the bubble collection process. b) A number of bubbles sticked on the bottom of small tank. c–g) Janus mesh with US-F surface facedown was used to absorb all the sticked bubbles and collect them into the small tube.

Figure 7 shows the bubble collecting process using the Janus stainless steel mesh fixed on a both-ends-open tube. S-F surface with superaerophilicity was toward tube, while US-F surface with ordinary aerophilicity was back to tube. Moving the device close to the bubbles on the bottom of the water sink, bubbles were absorbed by US-F surface and transformed to S-F surface gathering a gas pocket in tube. When the volume of gas on S-F surface was large enough to make its buoyancy overcome the adhesion force from surface, the gas escaped in the form of a bigger bubble into tube. Bubbles could be collected by the tube but could not run out reversely from it. Finally, all the bubbles in the water sink were collected in the tube (Figure 7g). The "bubble switch" may promote the design of advanced devices for application in pipe gas transportation and biological engineering.

3. Conclusions

In conclusion, underwater superaerophobicity/superaerophilicity and unidirectional passage were realized on stainless steel mesh by both-side and one-side femtosecond laser scanning and farther fluoroalkylsilane modification. The laser-structured both-side trinary-scale rough mesh was superhydrophilic in air and superaerophobic in water. After modification with a layer of fluoroalkylsilane by immersing into the 0.02% fluoroalkylsilane/ethanol solution for 24 h, the both-side rough mesh transferred to superhydrophobic in air and superaerophilic in water. When plenty of bubbles arrived at the surfaces, they could be absorbed and pass through the rough surface without fluorosilane treatment, while being intercepted by the rough surface with fluorosilane treatment. One-side rough mesh (Janus mesh) was fabricated by only structured one side of the stainless steel mesh and following fluorinated treatment. The structured side surface showed the underwater superaerophilicity while the unstructured side surface showed the underwater aerophilicity. No matter which surface is facing down, the bubbles can only penetrated from the US-F surface to S-F surface under the Laplace force. This unidirectional passage could be regarded as a "diode membrane" and eliminate the adhered bubbles at the bottom of the tank and collect them into the small tube.

4. Experimental Section

Femtosecond Laser Treatment: An AISI304 stainless steel mesh (300 mesh, a wire diameter of 40 µm) was previously cleaned with acetone, ethanol, and deionized water in an ultrasonic bath. The femtosecond laser pulses produced by a regenerative amplified Ti:sapphire laser system (CoHerent, Libra-usp 1 K-he-200) have the pulse width of 50 fs, center wavelength of 800 nm, and repetition frequency of 1 kHz. The laser beam was focused onto the stainless steel mesh surface by an objective lens (numerical aperture = 0.45, 20× Nikon), with the diameter of the focused laser beam of ≈10 µm. The typical "line-by-line" scanning method was adopted during femtosecond laser processing, which could refer to the previous works.[16,17] The laser power was set as constant at 27 mW. The scanning speed and the space of the scanning lines were adjusted by control program. After that the whole upper surface of the mesh was treated by laser, and the mesh was turned over to allow the laser beam to ablate another unablated side (Figure 1b). Finally, the laser-structured mesh was ultrasonically cleaned again.

Reducing the Surface Free Energy: To reduce the free energy of the mesh surface, the structured stainless steel mesh was immersed in a 0.2% 1*H*,1*H*,2*H*,2*H*-perfluorodecyltrimethoxysilane (Sigma–Aldrich) of ethanol solution at room temperature (≈20 °C) for 24 h. The fluoroalkylsilane molecular was spontaneously deposited on the surface of structured rough mesh. Then, the mesh was shifted to a vacuum oven and dried at 100 °C for 2 h to make the deposited fluoroalkylsilane layer more stable.

Characterization: The laser-induced surface microstructure of the stainless steel mesh was observed by a Quantan 250 FEG SEM (FEI, America). The EDX spectroscopy of the sample surfaces was obtained using the FEI Helios FIB/SEM 660. The WCA, WSA, underwater BCA,

and underwater bubble sliding angle (BSA) were measured by a JC2000D contact-angle measurement (Powereach, China). The volume of the used water droplet was 7 µL and that of bubble was 3 µL. The ultrafast processes of selective bubble passage and unidirectional bubble penetration were captured through a CAMMC1362 high-speed camera (Microtron, Germany) with a frame rate of 500 fps.

Supporting Information

Supporting Information is available from the Wiley Online Library or from the author.

Acknowledgements

This work was supported by the National Key Research and Development Program of China under the Grant No.2017YFB1104700, the National Science Foundation of China under the Grant Nos. 61875158 and 61805192, the International Joint Research Laboratory for Micro/Nano Manufacturing and Measurement Technologies, the Fundamental Research Funds for the Central Universities.

Conflict of Interest

The authors declare no conflict of interest.

Keywords

bubble passage, femtosecond laser, Janus mesh, underwater superaerophilicity, underwater superaerophobicity

Received: December 17, 2019
Revised: April 12, 2020
Published online:

[1] T. Cook, D. Dogutan, S. Reece, Y. Surendranath, T. Teets, D. Nocera, *Chem. Rev.* **2010**, *110*, 6474.
[2] Z. Lu, M. Sun, T. Xu, Y. Li, W. Xu, Z. Chang, Y. Ding, X. Sun, L. Jiang, *Adv. Mater.* **2015**, *27*, 2361.
[3] Z. Lu, W. Zhu, X. Yu, H. Zhang, Y. Li, X. Sun, X. Wang, H. Wang, J. Wang, J. Luo, X. Lei, L. Jiang, *Adv. Mater.* **2014**, *26*, 2683.
[4] C. Oliveira, R. Rodrigues, J. Rubio, *Bubble Sci., Eng., Technol.* **2014**, *5*, 15.
[5] R. Smart, A. Gerson, M. Biesinger, B. Hart, *Surf. Interface Anal.* **2017**, *49*, 1387.
[6] B. Albijanic, O. Ozdemir, A. Nguyen, D. Bradshaw, *Adv. Colloid Interface Sci.* **2010**, *159*, 1.
[7] Y. Li, H. Zhang, T. Xu, Z. Lu, X. Wu, P. Wan, X. Sun, L. Jiang, *Adv. Funct. Mater.* **2015**, *25*, 1737.
[8] R. Aben, *Nat. Commun.* **2017**, *8*, 1682.
[9] E. Stratakis, A. Ranella, C. Fotakis, *Biomicrofluidics* **2011**, *5*, 013411.
[10] P. Wall, O. McRae, V. Natarajan, C. Johnson, C. Antoniou, *Sci. Rep.* **2017**, *7*, 15102.
[11] P. Wall, J. Bird, L. Bourouiba, *Integr. Comp. Biol.* **2014**, *54*, 1014.
[12] R. Cherry, C. Hulle, *Biotechnol. Prog.* **1992**, *8*, 11.
[13] C. Yu, M. Cao, Z. Dong, K. Li, C. Yu, J. Wang, L. Jiang, *Adv. Funct. Mater.* **2016**, *26*, 6830.
[14] X. Chen, Y. Wu, B. Su, J. Wang, Y. Song, L. Jiang, *Adv. Mater.* **2012**, *24*, 5884.
[15] X. Lv, Y. Jiao, S. Wu, C. Li, Y. Zhang, J. Li, Y. Hu, D. Wu, *ACS Appl. Mater. Interfaces* **2019**, *11*, 20574.
[16] Y. Jiao, X. Lv, Y. Zhang, C. Li, J. Li, H. Wu, Y. Xiao, S. Wu, Y. Hu, D. Wu, J. Chu, *Nanoscale* **2019**, *11*, 1370.
[17] X. Xue, R. Wang, L. Lan, J. Wang, Z. Xue, L. Jiang, *ACS Appl. Mater. Interfaces* **2018**, *10*, 5099.
[18] H. Ma, M. Cao, C. Zhang, Z. Bei, K. Li, C. Yu, L. Jiang, *Adv. Funct. Mater.* **2018**, *28*, 1705091.
[19] C. Yu, X. Zhu, M. Cao, C. Yu, K. Li, L. Jiang, *J. Mater. Chem. A* **2016**, *4*, 16865.
[20] J. Yong, F. Chen, W. Li, J. Huo, Y. Fang, Q. Yang, H. Bian, X. Hou, *Global Challenges* **2018**, *2*, 1700133.
[21] J. Huo, J. Yong, F. Chen, Q. Yang, Y. Fang, X. Hou, *Adv. Mater. Interfaces* **2019**, *6*, 1900262.
[22] J. Yong, F. Chen, J. Huo, Y. Fang, Q. Yang, J. Zhang, X. Hou, *Nanoscale* **2018**, *10*, 3688.
[23] Y. Jiao, C. Li, X. Lv, Y. Zhang, S. Wu, C. Chen, Y. Hu, J. Li, D. Wu, *J. Mater. Chem. A* **2018**, *6*, 20878.
[24] J. Yong, F. Chen, M. Li, Q. Yang, Y. Fang, J. Huo, X. Hou, *J. Mater. Chem. A* **2017**, *5*, 25249.
[25] J. Yong, F. Chen, Y. Fang, J. Huo, Q. Yang, J. Zhang, H. Bian, X. Hou, *ACS Appl. Mater. Interfaces* **2017**, *9*, 39863.
[26] Y. Jiao, C. Li, S. Wu, Y. Hu, J. Li, L. Yang, D. Wu, J. Chu, *ACS Appl. Mater. Interfaces* **2018**, *10*, 16867.
[27] J. Yong, C. Subhash, Z. Zhan, F. Chen, C. Guo, *ACS Appl. Mater. Interfaces* **2019**, *11*, 8667.
[28] D. Gao, J. Cao, Z. Guo, *Chem. Commun.* **2019**, *55*, 3394.
[29] C. Shan, J. Yong, Q. Yang, F. Chen, J. Huo, J. Zhuang, Z. Jiang, X. Hou, *AIP Adv.* **2018**, *8*, 045001.
[30] C. Pei, Y. Peng, Y. Zhang, D. Tian, K. Liu, L. Jiang, *ACS Nano* **2018**, *12*, 5489.
[31] S. Yan, F. Ren, C. Li, Y. Jiao, C. Wang, S. Wu, S. Wei, Y. Hu, J. Li, Y. Xiao, Y. Su, D. Wu, *Appl. Phys. Lett.* **2018**, *113*, 261602.
[32] S. Wu, D. Meng, C. Chen, L. Shi, L. Zhou, Z. Huang, J. Li, Y. Hu, D. Wu, *Adv. Mater. Interfaces* **2019**, *6*, 1901176.
[33] C. Chen, L. Shi, Z. Huang, Y. Hu, S. Wu, J. Li, D. Wu, J. Chu, *Adv. Mater. Interfaces* **2019**, *6*, 1900297.
[34] J. Yong, F. Chen, Q. Yang, Z. Jiang, X. Hou, *Adv. Mater. Interfaces* **2018**, *5*, 1701370.
[35] K. Sugioka, Y. Cheng, *Light: Sci. Appl.* **2014**, *3*, e149.
[36] F. Chen, D. Zhang, Q. Yang, J. Yong, G. Du, J. Si, F. Yun, X. Hou, *ACS Appl. Mater. Interfaces* **2013**, *5*, 6777.
[37] T. Chong, M. Hong, L. Shi, *Laser Photonics Rev.* **2010**, *4*, 123.
[38] J. Yong, J. Huo, Q. Yang, F. Chen, Y. Fang, X. Wu, L. Liu, X. Lu, J. Zhang, X. Hou, *Adv. Mater. Interfaces* **2018**, *5*, 1701479.
[39] K. Sugioka, Y. Cheng, *Appl. Phys. Rev.* **2014**, *1*, 041303.
[40] M. Li, M. Liu, H. Sun, *Phys. Chem. Chem. Phys.* **2019**, *21*, 24262.
[41] Y. Liu, D. Han, Z. Jiao, Y. Liu, H. Jiang, X. Wu, H. Ding, Y. Zhang, H. Sun, *Nanoscale* **2017**, *9*, 17933.
[42] B. Wu, M. Zhou, J. Li, X. Ye, G. Li, L. Cai, *Appl. Surf. Sci.* **2009**, *256*, 61.
[43] A. Vorobyev, C. Guo, *Opt. Express* **2006**, *14*, 2164.
[44] S. Hou, Y. Huo, P. Xiong, Y. Zhang, S. Zhang, T. Jia, Z. Sun, J. Qiu, Z. Xu, *J. Phys. D: Appl. Phys.* **2011**, *44*, 505401.
[45] S. Amoruso, G. Ausanio, R. Bruzzese, M. Vitiello, X. Wang, *Phys. Rev. B* **2005**, *71*, 033406.

